Progress In Electromagnetics Research, Vol. 155, 115–125, 2016

Wideband Multifunctional Metasurface for Polarization Conversion and Gain Enhancement

Hai-Peng Li*, Guang-Ming Wang, Jian-Gang Liang, and Xiang-Jun Gao

Abstract—We propose a wideband multifunctional device which combines a linear-to-circular polarization convertor with focusing metasurface. The proposed design is built by a novel dual-layered metal cross and cross ring unit cell which exhibits satisfying performance for controlling the reflecting phase of the electromagnetic wave polarization-independently. The device is illuminated by a Vivaldi antenna, and the functions of polarization conversion and gain enhancement have been simultaneously achieved in the band of 9.12–10.2 GHz. In addition, the polarization helicity of the system can be reconfigured by rotating the feed antenna. The device has not only greatly presented the flexibility and superiority of the metasurface in steering the electromagnetic waves, but also promoted the development of the multifunctional metasurface.

1. INTRODUCTION

Metamaterials are artificial materials that possess peculiar properties not found in nature [1–4]. Recently, metasurfaces (MSs) [5–25] — two-dimensional version of metamaterials — have become a research hotspot because of their extraordinary properties with the advantage of easy fabrication, compactness, and low loss. A MS usually consists of a set of subwavelengh resonant structures with different geometrical parameters. It can manipulate the scattering EM waves with controlled amplitude and phase and thus possesses special functionalities such as anomalous reflection/refraction and polarization conversion provided that these constitutive unit cells are carefully arranged on a surface. Thereinto, the polarization state is one of the most important characteristics of the EM waves. We can classified the polarization conversion MS (PCMS) [14–19] into two categories according to the format of the MS — transmitting type [14–17] and reflecting type [18, 19]. Also, the PCMS also can be classified into cross-polarization conversion one [14–16, 18] or linear-to-circular/circular-to-linear (LTC/CTL) one [17, 19] according to specific functionalities. However, the mentioned PCMSs are all illuminated by plane waves and the radiation performances will be more or less deteriorated when they are directly feed by a spherical feed source like Vivaldi antenna. Taking the overall performances into consideration, a technique should be adopted for a PCMS design to control the direction of the scattering wave for spherical wave excitation.

The phase gradient metasurface (PGMS), firstly proposed by Yu et al. [5], is a special kind of MS which enables to provide pre-defined in-plane wave vectors to manipulate the directions of the refracting/reflecting waves. In that article, the PGMS was utilized to demonstrate the general Snell's law by using nano-V-antennas with different shapes, which opens the door to the rapid development of MS for beam steering such as anomalous refraction/reflection and focusing. Among them, the focusing MS [18–23] can transfer the incident plane wave to its focal point, and vice versa. So it can be predicted that the combination of the PCMS with focusing MS will improve the radiation performance of the system.

Received 20 January 2016, Accepted 19 March 2016, Scheduled 23 March 2016
* Corresponding author: Hai-Peng Li (s_lihaipeng@sina.com).
The authors are with the Air and Missile Defense College, Air force Engineering University, Xi'an, Shaanxi Province 710051, China.

In this paper, we design a multifunctional reflected MS by combining a linear-to-circular polarization convertor and a focusing metasurface. A Vivaldi antenna operating in a wideband has been designed for illuminating the MS. Simultaneously, the new MS can achieve polarization conversion with radiation improvement in a wide band. The MS is built by a novel unit cell which consists of a dual-layered metal cross and cross ring (CCR) to cover $[0,\ 2\pi]$ phase change. Comparing with LTC-MS, the multifunctional MS enhance the gain and decrease beam width of the antenna in a 3 dB AR band of 9.12–10.2 GHz. As the rotation of the antenna, a reflecting wave with x polarization, left-handed circular polarization (LHCP), y polarization or right-handed circular polarization (RHCP) can be obtained respectively. To demonstrate the proposed scheme, a finally designed MS, occupying an area of 130 mm × 130 mm, has been fabricated using PCB technics and measured in a anechoic chamber. The proposed design is not only an improvement to the PCMS but also a promotion for the multifuctional MS development.

2. LTC-PCMS DESIGN

Anisotropic structures have the potential to manipulate electromagnetic waves with different polarizations respectively. The structure of the proposed anisotropic MS unit cell is shown in Fig. 1, the unit cell consists of a metal cross and metal cross ring (CCR) on a substrate board with a permittivity of 2.65. The unit cell is simulated in CST Microwave Studio by using periodic boundary in x and y direction, see simulation setup shown in Fig. 1(b). We set r_x and r_y with different values to make the reflecting phase change with the polarization of the incident wave. The reflection matrix (R matrix), which connects the incident fields and reflected fields, can be described as

$$R = \begin{pmatrix} R_{xx} & R_{yx} \\ R_{xy} & R_{yy} \end{pmatrix} \tag{1}$$

where R_{ij} represents the reflection coefficient of j polarization incident wave and i polarization reflected wave. When $r_x = 4.06$ mm and $r_y = 3.6$ mm, the simulation results in Fig. 2 show that $\mathrm{Am}(R_{xx}) = \mathrm{Am}(R_{yy}) = 1$, $\mathrm{Am}(R_{yx}) = \mathrm{Am}(R_{xy}) = 0$ and $\mathrm{Arg}(R_{xx}) - \mathrm{Arg}(R_{yy}) \approx -90^\circ$ in the band of 9.1–10.3 GHz. In this situation, the R matrix is:

$$R = \begin{pmatrix} -j & 0 \\ 0 & 1 \end{pmatrix} e^{-j\varphi} \tag{2}$$

To not lose the generality, we suppose that the LTC-PCMS is illuminated by a plane wave propagating along $-z$ direction, then we have

$$\vec{E}_i = (\hat{x}E_x + \hat{y}E_y)\, e^{-jkz} \tag{3}$$

$$\begin{pmatrix} E_x \\ E_y \end{pmatrix} = \begin{pmatrix} \cos\theta \\ \sin\theta \end{pmatrix} e^{-jkz} \tag{4}$$

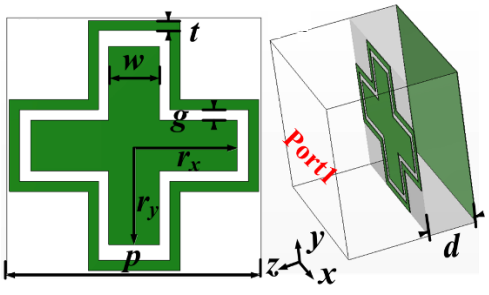

Figure 1. Topology of the proposed LTC-PCMS unit cell with $g = t = 0.4$ mm, $p = 10$ mm, $d = 3$ mm, $w = 2.4$ mm. (a) Front view; (b) perspective view. The metallic is shown in green while the slot is shown in white.

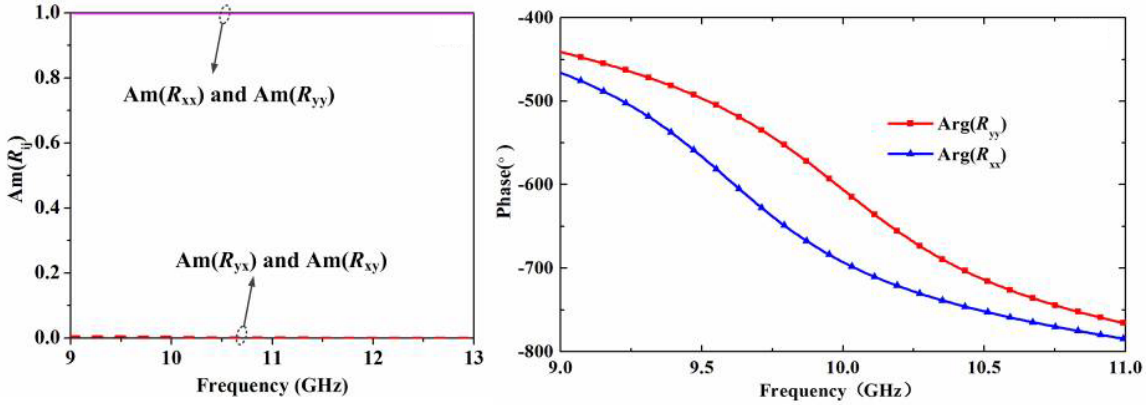

(a) (b)

Figure 2. The (a) amplitudes and (b) angles of the R matrix.

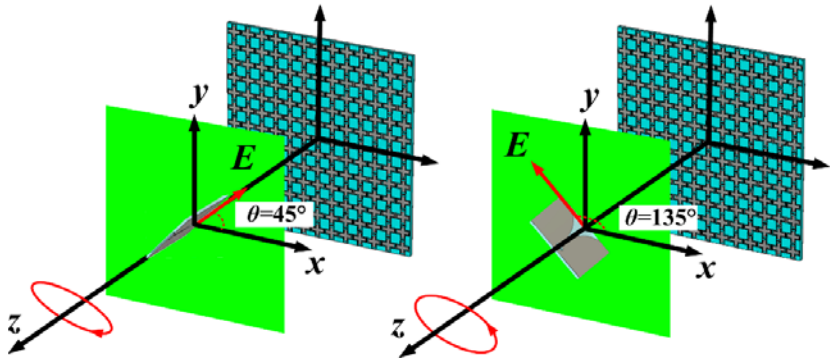

(a) (b)

Figure 3. The scheme of proposed two situations for different E field directions at (a) $\theta = 45°$ and (b) $\theta = 135°$.

where k is the wave number. In the following, we will discuss that our LTC-PCMS supports linear wave to LHCP or RHCP wave conversion in two special cases.

In the first case of $\theta = 45°$, the incident E fields can be calculated as

$$\begin{pmatrix} E_x \\ E_y \end{pmatrix} = \frac{\sqrt{2}}{2} \begin{pmatrix} 1 \\ 1 \end{pmatrix} e^{-jkz} \tag{5}$$

then the reflected E fields can be calculated as:

$$\begin{pmatrix} E_{rx} \\ E_{ry} \end{pmatrix} = R\frac{\sqrt{2}}{2} \begin{pmatrix} 1 \\ 1 \end{pmatrix} e^{jkz} e^{-j\varphi} = \frac{\sqrt{2}}{2} \begin{pmatrix} -j \\ 1 \end{pmatrix} e^{jkz} e^{-j\varphi} \tag{6}$$

$$\vec{E}_r = E_{rx}\hat{x} + E_{ry}\hat{y} = \frac{\sqrt{2}}{2} \left(-j\hat{x} + \hat{y}\right) e^{jkz} e^{-j\varphi} \tag{7}$$

From Eq. (6), it can be concluded that a LHCP reflected wave can be obtained in this situation as shown in Fig. 3(a).

In the second case of $\theta = 135°$, we can obtain following results by taking similar calculations:

$$\vec{E}_r = E_{rx}\hat{x} + E_{ry}\hat{y} = \frac{\sqrt{2}}{2} \left(j\hat{x} + \hat{y}\right) e^{jkz} e^{-j\varphi} \tag{8}$$

In this situation, a RHCP reflected wave has been obtained.

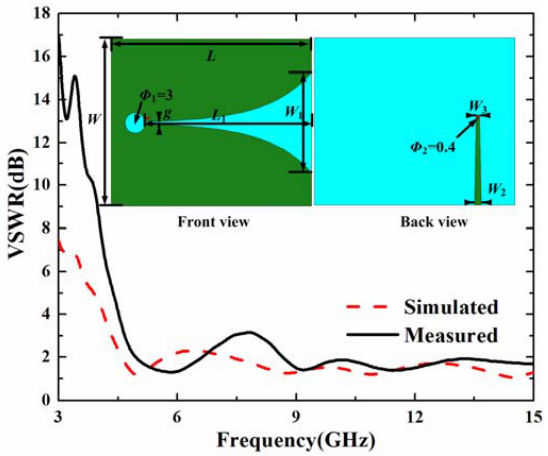

Figure 4. The VSWR of the Vivaldi antenna. The geometrical parameters are $W = 25\,\text{mm}$, $L = 30\,\text{mm}$, $L_1 = 25\,\text{mm}$, $W_1 = 15\,\text{mm}$, $W_2 = 1\,\text{mm}$, $W_3 = 0.5\,\text{mm}$, $g = 0.5\,\text{mm}$, $\Phi_1 = 3\,\text{mm}$ (the diameter of the cicular slot end), $\Phi_2 = 0.4\,\text{mm}$ (the diameter of the metallic through hole).

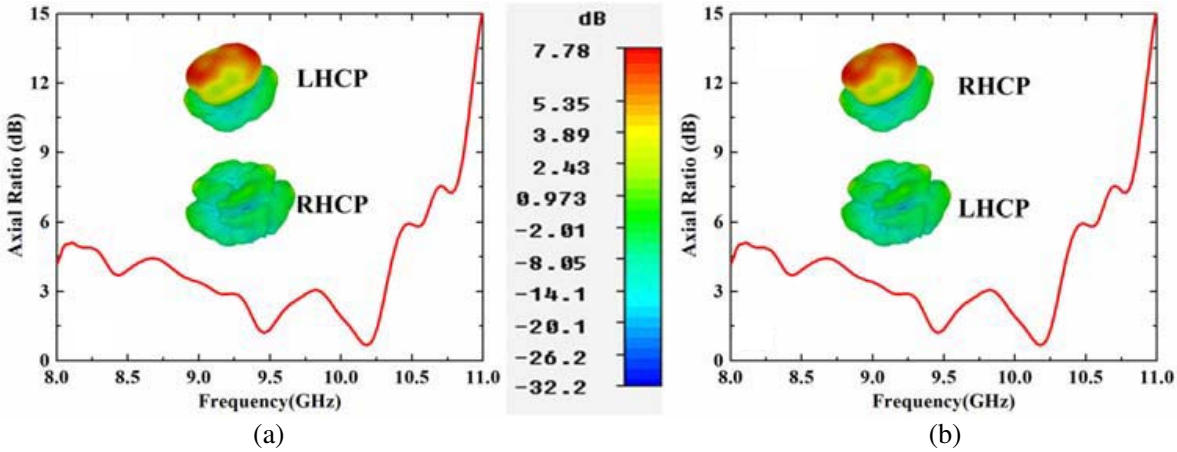

Figure 5. 3D radiation patterns and AR results of the LTC-PCMS for (a) $\theta = 45°$ and (b) $\theta = 135°$ at 10 GHz.

To verify above prediction, Fig. 3 depicts a practical realized scheme of our system, where the LTC-PCMS composed of 13×13 single-layered CCR unit cells is fed by a Vivaldi antenna. The antenna has been rotated around its own axis with 45° and 135° respectively, and it is placed 60 mm away from the MS. Fig. 4 shows the voltage standing wave ratio (VSWR) and also the geometrical parameters of the Vivaldi antenna.

The antenna 3D radiation patterns and AR of the LTC-PCMS for the two situations are depicted in Fig. 5. It is shown that the 3 dB AR bandwidth covers 9.1–10.3 GHz and the results are the same except that the co-polarization is LHCP for $\theta = 45°$ while it is RHCP for $\theta = 135°$. Therefore, our proposed scheme and design has been successfully verified. Despite this, it also should be noted that the radiation pattern of the Vivaldi antenna deteriorates to some degree with the polarization conversion, which can be depicted more clearly by the comparison of 2D ridiation patterns with and without the LTC-PCMS shown in Fig. 6. As shown, not only the peak gain decreases but also the beam width expands when the LTC-MS exists. To solve the problem, we introduce a focusing MS to collimate the phase of the aperture field and thus improve the radiation performances.

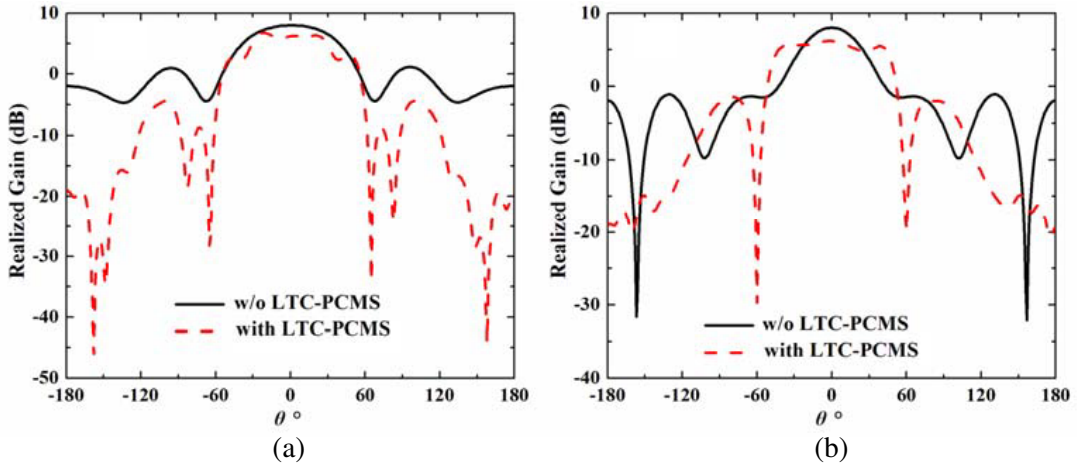

Figure 6. The 2D co-polarization radiation patterns at 10 GHz of the Vivaldi antenna with and without the LTC-PCMS. (a) xoz plane, (b) yoz plane.

3. MULTIFUNCTIONAL MS DESIGN

To ease the design, the unit cell should exhibit polarization-independent electrical response, and the phase changing range should cover $[0, 2\pi]$. By simulations, we find that the single-layered CCR element features good polarization-independent reflected phase responses by tuning the length of the cross r_x and r_y but still lacks sufficient phase changing range. However, a dual-layered CCR element is a perfect alternative and is adopted for our design.

The dual-layered element has the same parameters with the single-layered one, and the phases of S_{11} for x/y polarization are shown Fig. 7, where d indicates the thickness of the substrate. It is shown that the parameter $r_x(r_y = 4.06\,\text{mm})$ just affects the value of $\text{Arg}(R_{xx})$ while $\text{Arg}(R_{yy})$ is almost constant when r_x increases from 2.3 mm to 4.06 mm. Meanwhile, the phase variation range of $\text{Arg}(R_{xx})$ has reached 360°. Since the CCR unit cell exhibits rotational symmetry, similar conclusion can be readily obtained when r_y is tuned while keep r_x constant. To demonstrate that the dual-layered CCR unit cell can manipulate the different polarization waves independently, a supercell with inverse linear phase gradient along x direction for x and y polarization has been designed. As shown in Fig. 8(a), the proposed supercell is composed of seven unit cells with the parameters of $r_{x1} = r_{y7} = 4.06\,\text{mm}$, $r_{x2} = r_{y6} = 3.95\,\text{mm}$, $r_{x3} = r_{y5} = 3.84\,\text{mm}$, $r_{x4} = r_{y4} = 3.67\,\text{mm}$, $r_{x5} = r_{y3} = 3.26\,\text{mm}$, $r_{x6} = r_{y2} = 2.62\,\text{mm}$, $r_{x7} = r_{y1} = 2.32\,\text{mm}$. For x polarization incident wave the step of the phase

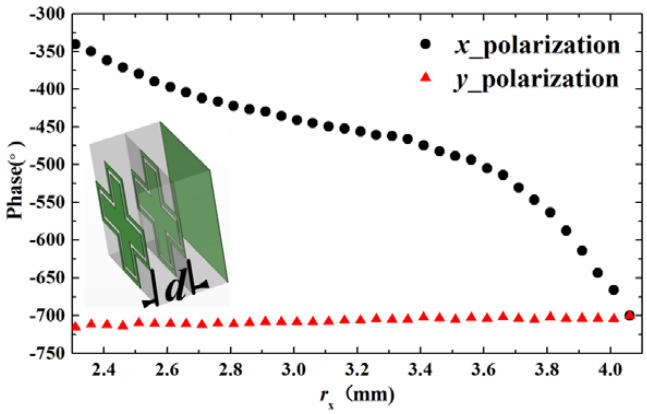

Figure 7. Phases of S_{11} for x/y polarizations of the dual-layered CCR unit cell with its structure.

difference is $+60^\circ$ along $+x$ direction while for y polarization the step is -60°. According to the generalized reflection law described in Eq. (9), the reflected wave will always deflect to the phase delay direction.

$$\sin(\theta_r) - \sin(\theta_i) = \frac{\lambda}{2\pi n_i}\frac{d\varphi}{dx} \tag{9}$$

where φ is the phase discontinuity at a local position on the MS, n_i the refractive index of the incident medium, $\theta_r(\theta_i)$ the reflected (incident) angle of the electromagnetic wave, and λ the wavelength. The supercell is simulated by using periodic boundary in y direction and open boundaries in x and z directions. So we can obtain that $d\varphi/dx = 2\pi/(Np - p)$, where N is the number of unit cells used for building the supercell. In the design, the sample is placed in free space (i.e., $n_i = 1$), thus θ_r can be obtained by Eq. (10).

$$\theta_r = \sin^{-1}\left[\frac{\lambda}{2\pi} \times \frac{2\pi}{(N-1)p}\right] \tag{10}$$

The anomalous reflections of the supercell are shown in Figs. 8(b) and (c), and we can find that the the reflected wave deflects to $-x(+x)$ direction with the angle of $\theta_{rx} \approx 30^\circ$ ($\theta_{ry} \approx 30^\circ$) when incident wave is $x(y)$ polarization. The simulation results have a good agreement with the theoretical calculations. The performances of the supercell verify that the dual-layered CCR element can steer the EM waves with different polarizations independently. To be specific, the phases of x and y polarization incident waves are controlled by r_x and r_y respectively and they do not influence each other. Therefore, design of the following multifunctional MS will be greatly simplified.

Firstly, for designing focusing MS the phase difference distribution on the MS has to satisfy Eq. (11).

$$\Delta\varphi(m,n) = \frac{2\pi}{\lambda}\left(\sqrt{(mp)^2 + (np)^2 + L^2} - L\right) \pm 2k\pi \quad (k = 0, 1, 2\ldots) \tag{11}$$

where L is the focal distance, $m(n)$ the number of the unit cell in $x(y)$ direction, and $\Delta\varphi(m,n)$ the phase difference according to the unit cell placed at the origin point ($m = 0$, $n = 0$).

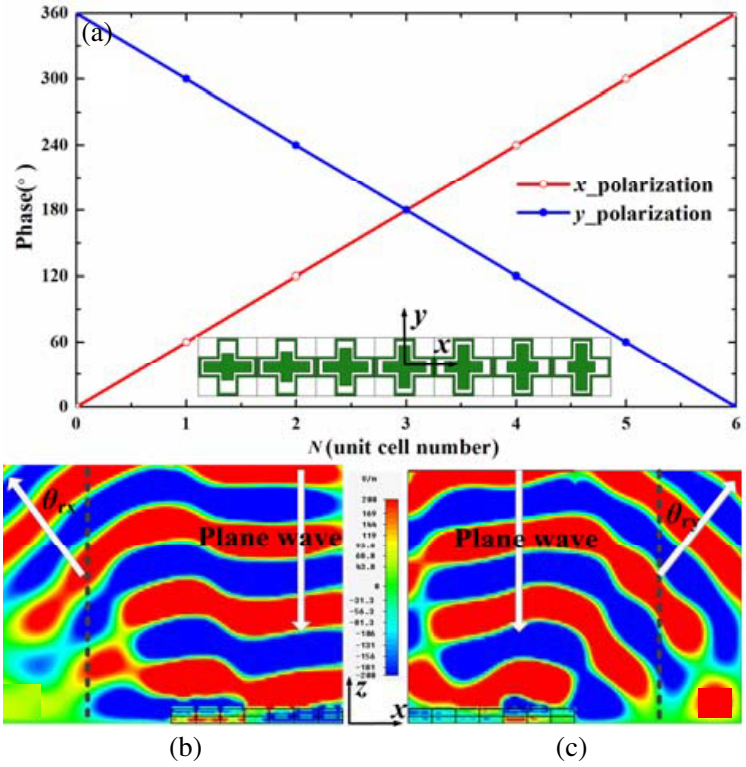

Figure 8. (a) Structure of the supercell and the phase difference distributions along x direction for x/y polarization and anomolous reflection for (b) x polarization and (c) y polarization incident wave.

Secondly, the phase delay for x polarization incident wave must have a 90° difference with the y polarization through each unit cell, namely $\mathrm{Arg}(R_{xx})_{mn} - \mathrm{Arg}(R_{yy})_{mn} \approx -90°$. $\mathrm{Arg}(R_{xx})_{mn}$ is controlled by the parameter of r_x while $\mathrm{Arg}(R_{yy})_{mn}$ is controlled by the parameter of r_y. For x polarization incident wave, the phase distribution can be deduced as:

$$\begin{aligned} \mathrm{Arg}(R_{xx})_{mn} - \mathrm{Arg}(R_{xx})_{00} &= \frac{2\pi}{\lambda}\left(\sqrt{(mp)^2 + (np)^2 + L^2} - L\right) \pm 2k\pi \\ &= \Delta\varphi_{xx}(m,n) \quad (k = 0, 1, 2\ldots) \end{aligned} \tag{12}$$

For y polarization incident wave, the phase distribution is:

$$\begin{aligned} \mathrm{Arg}(R_{yy})_{mn} - \mathrm{Arg}(R_{yy})_{00} &= \frac{2\pi}{\lambda}\left(\sqrt{(mp)^2 + (np)^2 + L^2} - L\right) \pm 2k\pi \\ &= \Delta\varphi_{yy}(m,n) \quad (k = 0, 1, 2\ldots) \end{aligned} \tag{13}$$

where, in the focusing LTC-PCMS design following equations have to be satisfied: $\mathrm{Arg}(R_{xx})_{00} - \mathrm{Arg}(R_{yy})_{00} \approx -90°$, $\Delta\varphi_{xx}(m,n) \in [0°, 360°]$, $\Delta\varphi_{yy}(m,n) \in [-90°, 270°]$. We fix $L = 2\lambda$, by insertion of $p = 10\,\mathrm{mm}$, $\lambda = 30\,\mathrm{mm}$, $\mathrm{Arg}(R_{xx})_{00} = -700°$, the phase distributions for the two polarizations are calculated by Eqs. (12) and (13), respectively, and then the values of r_x and r_y at each position (m, n) on the MS can be ascertained by Fig. 7 based on the calculated phase distributions. Fig. 9 shows the absolute phase distributions for the two polarizations, and Fig. 10 shows the parameter distributions.

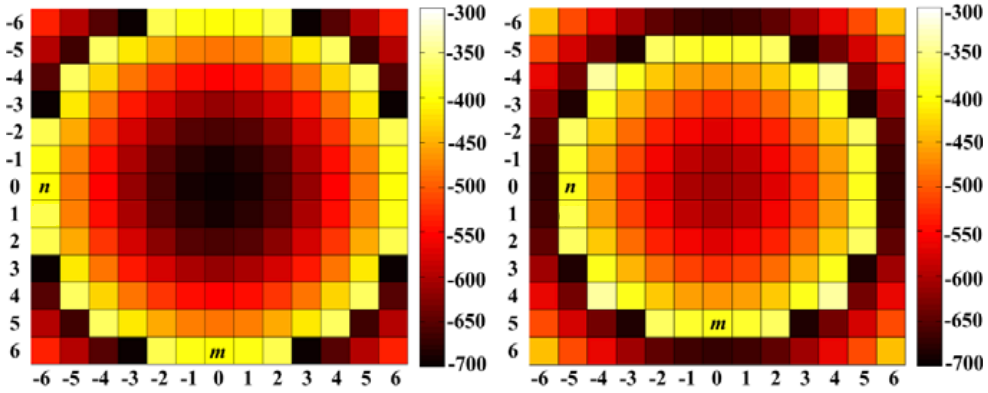

Figure 9. Absolute phase distributions for (a) x polarization and (b) y polarization.

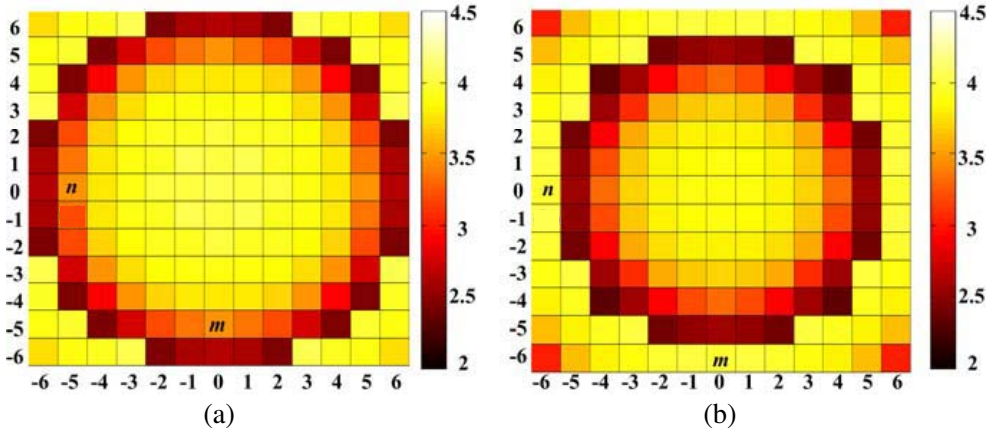

Figure 10. Distributions of (a) r_x and (b) r_y on the multifunctional MS.

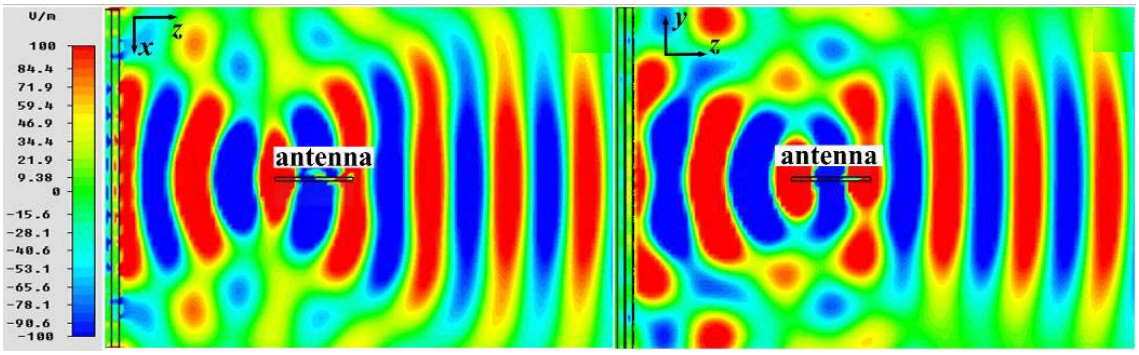

(a) (b)

Figure 11. Electric field distributions in (a) *xoz* and (b) *yoz* plane at 10 GHz.

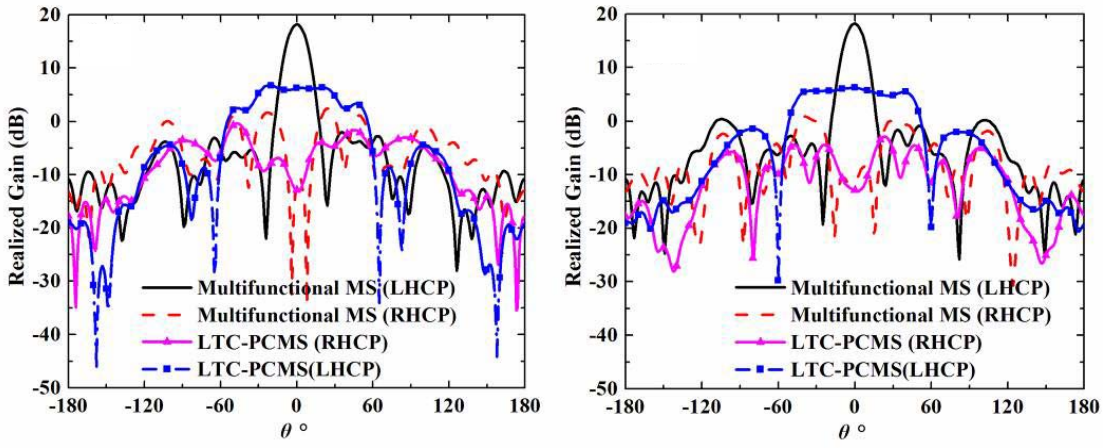

(a) (b)

Figure 12. 2D radiation patterns at 10 GHz. (a) *xoy*-plane, (b) *yoz*-plane.

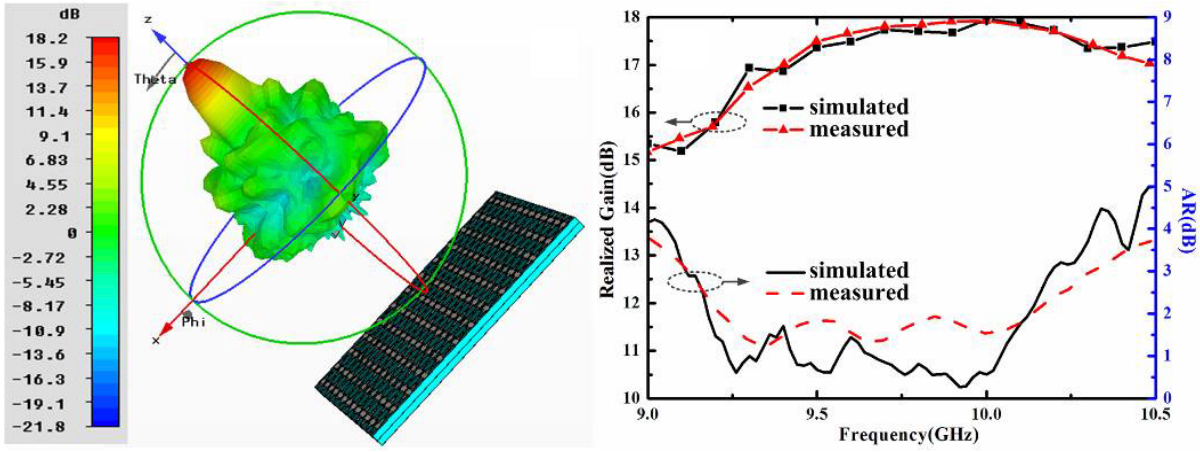

(a) (b)

Figure 13. (a) 3D ridiation pattern at 10 GHz, (b) simulated and measured results of axis ratios and realized gains.

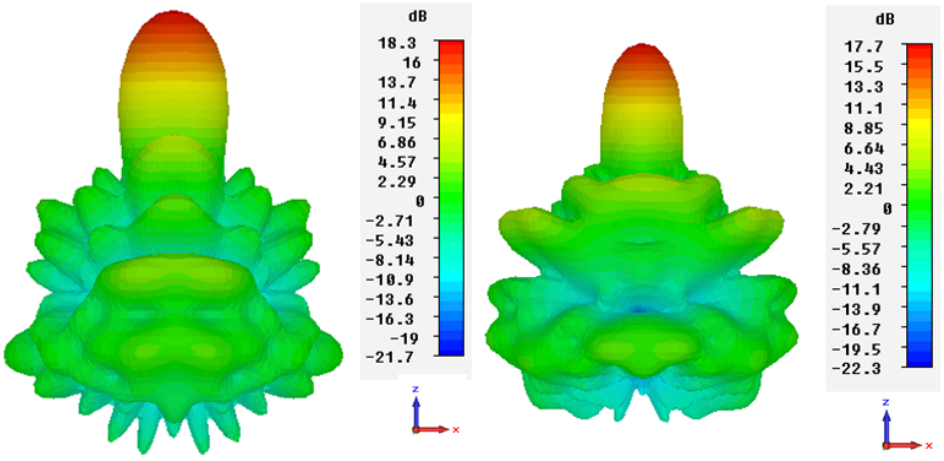

Figure 14. 3D radiation patterns at 10 GHz for (a) $\theta = 0°$ and (b) $\theta = 90°$.

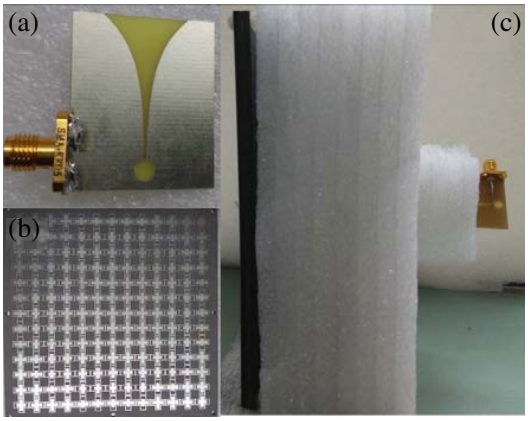

Figure 15. Photographs of the fabricated sample. (a) Vivaldi antenna, (b) multifunctional MS, (c) whole system.

Lastly, the proposed MS model is built in CST based on the matrixes of r_x and r_y, and a Vivaldi antenna is placed 60 mm away from MS as a the feed source. As shown in Fig. 3(a), we first set $\theta = 45°$, and a LHCP reflected wave will be obtained consequently. Fig. 11 describes the near-field electric field distributions in *xoz* and *yoz* plane, and it is shown that the reflected wave has been transformed to near-plane wave which is a extraordinary performance of focusing MS. The 2D patterns of *xoz* and *yoz* are shown in Fig. 12, and the pencil-shaped 3D radiation pattern and realized gains with AR results are shown in Fig. 13. Compared with LTC-PCMS, the new multifunctional MS enhances the gain and decreases beam width of the antenna in 3 dB AR band of 9.12–10.2 GHz. Specially, the realized gain has been enhanced 12 dB, and a half power beam width of 13° has been achieved at 10 GHz.

In addition, the models of $\theta = 0°$, 90° and 135° have also been simulated. It is similar to the LTC-PCMS, and the results for $\theta = 135°$ and 45° are the same except that the co-polarization is LHCP for $\theta = 45°$ while it is RHCP for $\theta = 135°$. For $\theta = 0°$, a x linear co-polarization reflected wave is obtained as shown in Fig. 14(a). On the other hand, for $\theta = 90°$, a y linear co-polarization reflected wave is obtained as shown in Fig. 14(b). So the whole system is polarization-reconfigurable to some extent. Finally, photographs of the fabricated sample are shown Fig. 15.

4. CONCLUSIONS

We have firstly simulated a single-layered LTC-PCMS feed by a Vivaldi antenna and analyze its farfield results. Then a dual-layered multifunctional MS has been proposed to simultaneously enhance the gain of the antenna and achieve linear-to-circular polarization conversion. The proposed CCR unit cell can manipulate different polarizations independently, and the phase discontinuities can be tuned flexibly in a whole range of 0 to 2π. The new MS enhances the gain and decreases beam width of the antenna in 3 dB AR band of 9.12–10.2 GHz. This work is a good combination of PCMS and focusing MS, and the polarization of the system is reconfigurable mechanically. The device not only presents the flexibility and superiority of the MS in manipulating EM waves, but also promotes the development of multifunctional MS.

ACKNOWLEDGMENT

This work is supported by the National Natural Science Foundation of China under Grant No. 61372034 and No. 61501499.

REFERENCES

1. Veselago, V. G., "The electrodynamics of substances with simultaneously negative values of ε and μ," *Soviet Physics Uspekhi*, Vol. 10, No. 4, 509–514, 1968.
2. Shelby, R. A., D. R. Smith, and S. Schultz, "Experimental verification of a negative index of refraction," *Science*, Vol. 292, No. 6, 77–79, 2001.
3. Xu, H.-X., G.-M. Wang, M. Q. Qi, T. Cai, and T. J. Cui, "Compact dual-band circular polarizer using twisted Hilbert-shaped chiral metamaterial," *Optics Express*, Vol. 21, No. 21, 24912–24921, 2013.
4. Xu, H.-X., G.-M. Wang, M.-Q. Qi, and T. Cai, "Dual-band circular polarizer and asymmetric spectrum filter using ultrathin compact chiral metamaterial," *Progress In Electromagnetics Research*, Vol. 143, 243–261, 2013.
5. Yu, N. F., P. Genevet, M. A. Kats, F. Aieta, J.-P. Tetienne, F. Capasso, and Z. Gaburro, "Light propagation with phase discontinuities: Generalized laws of reflection and refraction," *Science*, Vol. 334, 333–337, 2011.
6. Ni, X., N. K. Emani, A. V. Kildishev, A. Boltasseva, and V. M. Shalaev, "Broadband light bending with plasmonic nanoantennas," *Science*, Vol. 335, 427, 2012.
7. Sun, S. L., Q. He, S. Y. Xiao, Q. Xu, X. Li, and L. Zhou, "Gradient-index meta-surfaces as a bridge linking propagating waves and surface waves," *Nature Mater.*, Vol. 11, 426–431, 2012.
8. Zhao, J. J., B. W. Li, Z. N. Chen, and C. W. Qiu, "Redirection of sound waves using acoustic metasurface," *Appl. Phys. Lett.*, Vol. 103, 151604, 2013.
9. Yang, Q. L., J. Q. Gu, D. Y. Wang, X. Q. Zhang, Z. Tian, C. M. Ouyang, R. Singh, J. G. Han, and W. L. Zhang, "Efficient flat metasurface lens for terahertz imaging," *Opt. Express*, Vol. 22, No. 21, 25931–25939, 2014.
10. Pors, A. and S. I. Bozhevolnyi, "Plasmonic metasurfaces for efficient phase control in reflection," *Opt. Express*, Vol. 21, No. 22, 27438–27451, 2013.
11. Wei, Z. Y., Y. Cao, X. P. Su, Z. J. Gong, Y. Long, and H. Q. Li, "Highly efficient beam steering with a transparent metasurface," *Opt. Express*, Vol. 21, No. 9, 10739–10745, 2013.
12. Pfeiffer, C., N. K. Emani, A. M. Shaltout, et al., "Efficient light bending with isotropic metamaterial Huygens' surfaces," *Nano Lett.*, Vol. 14, No. 5, 2491–2497, 2014.
13. Farahani, M. F. and H. Mosallaei, "Birefringent reflectarray metasurface for beam engineering in infrared," *Opt. Lett.*, Vol. 38, No. 4, 462–464, 2013.
14. Song, K., Y. H. Liu, C. R. Luo, and X. P. Zhao, "High-efficiency broadband and multiband cross-polarization conversion using chiral metamaterial," *J. Phys. D: Appl. Phys.*, Vol. 47, 505104, 2014.

15. Yang, Y. M., W. Y. Wang, P. Moitra, I. I. Kravchenko, D. P. Briggs, and J. Valentine, "Dielectric meta-reflectarray for broadband linear polarization conversion and optical vortex generation," *Nano Lett.*, Vol. 14, 1394–1399, 2014.
16. Grady, N. K., J. E. Heyes, D. R. Chowdhury, Y. Zeng, et al., "Terahertz metamaterials for linear polarization conversion and anomalous refraction," *Science*, Vol. 340, 1304–1306, 2013.
17. Zhu, L., F.-Y. Meng, L. Dong, J.-H. Fu, F. Zhang, and Q. Wu, "Polarization manipulation based on electromagnetically induced transparency-like (EIT-like) effect," *Opt. Express*, Vol. 21, No. 26, 32100–32110, 2013.
18. Chen, H. Y., J. F. Wang, H. Ma, S. B. Qu, Z. Xu, A. X. Zhang, M. B. Yan, and Y. F. Li, "Ultra-wideband polarization conversion metasurfaces based on multiple plasmon resonances," *J. Appl. Phys.*, 154504, 2014.
19. Ma, H. F., G. Z. Wang, G. S. Kong, and T. J. Cui, "Broadband circular and linear polarization conversions realized by thin birefringent reflective metasurfaces," *Opt. Mater. Express*, Vol. 4, No. 8, 1718–1724, 2014.
20. Pors, A., M. G. Nielsen, R. L. Eriksen, and S. I. Bozhevolnyi, "Broadband focusing flat mirrors based on plasmonic gradient metasurfaces," *Nano Lett.*, Vol. 13, 829–834, 2013.
21. Li, X., S. Y. Xiao, B. G. Cai, Q. He, T. J. Cui, and L. Zhou, "Flat metasurfaces to focus electromagnetic waves in reflection geometry," *Opt. Lett.*, Vol. 37, No. 23, 4940–4942, 2012.
22. Aieta, F., P. Genevet, M. A. Kats, N. F. Yu, R. Blanchard, Z. Gaburro, and F. Capasso, "Aberration-free ultrathin flat lenses and axicons at telecom wavelengths based on plasmonic metasurfaces," *Nano Lett.*, Vol. 12, 4932–4936, 2012.
23. Monticone, F., N. M. Estakhri, and A. Alù, "Full control of nanoscale optical transmission with a composite metascreen," *Phys. Rev. Lett.*, Vol. 110, 203903, 2013.
24. Chen, J., Q. Cheng, J. Zhao, D. S. Dong, and T.-J. Cui, "Reduction of radar cross section based on a metasurface," *Progress In Electromagnetics Research*, Vol. 146, 71–76, 2014.
25. Cheng, J. and H. Mosallaei, "Optical metasurfaces for beam scanning in space," *Opt. Lett.*, Vol. 39, No. 9, 2719–2722, 2014.